Journal of Alloys and Compounds 502 (2010) 92–96

Contents lists available at ScienceDirect

Journal of Alloys and Compounds

journal homepage: www.elsevier.com/locate/jallcom

Structural and electrochemical properties of Al^{3+} doped V_2O_5 nanoparticles prepared by an oxalic acid assisted soft-chemical method

Shiying Zhan [a], Yingjin Wei [b,*], Xiaofei Bie [a], Chunzhong Wang [b], Fei Du [b], Gang Chen [b], Fang Hu [a]

[a] College of Materials Science and Engineering, Jilin University, Changchun 130012, China
[b] College of Physics and State Key Laboratory of Superhard Materials, Jilin University, Changchun 130012, China

ARTICLE INFO

Article history:
Received 16 August 2009
Received in revised form 15 March 2010
Accepted 16 March 2010
Available online 20 March 2010

Keywords:
Nanostructured materials
V_2O_5
Raman scattering
Electrochemistry
Rechargeable lithium batteries

ABSTRACT

V_2O_5 and $Al_{0.2}V_2O_5$ nanoparticles were prepared by an oxalic acid assisted soft-chemical method. X-ray photoelectron spectroscopy confirmed the V^{5+} oxidation state of V_2O_5, whereas an intermediate state between V^{5+} and V^{4+} of $Al_{0.2}V_2O_5$. Raman scattering showed that the Al^{3+} ions existed in an $[AlO_6]$ octahedral environment. The doping of Al^{3+} increased the cohesion between the V_2O_5 slabs, which enhanced the structural stability of the material. The chemical diffusion coefficients of the $Al_{0.2}V_2O_5$ nanoparticles were a little bit smaller than those of V_2O_5. Charge–discharge cycling showed that the $Al_{0.2}V_2O_5$ nanoparticles exhibited much better capacity retention than the un-doped V_2O_5, which was attributed to the enhanced structural stability of the material.

1. Introduction

Vanadium oxides (e.g. VO_2, V_6O_{13} and V_2O_5) are potential cathode materials for rechargeable lithium batteries [1–3]. Among these materials, V_2O_5 is probably the most studied one due to its unique features such as easy preparation, low cost, high stability and large energy density [4]. However, it is well known that pristine bulk V_2O_5 is not an appropriate cathode material because of its low lithium diffusion coefficient and poor structural stability with lithium insertion/extraction, which lead to bad battery performance such as poor capacity retention and low rate capability. Recently, many studies have been focused on the composite or novel structured V_2O_5 cathode materials [5–8]. Especially, the nanostructured materials exhibit better electrochemical performance with respect to bulk V_2O_5 by virtue of their morphology properties. The small size of these materials can boost redox reactivity and their short diffusion pathways enable the materials to withstand high discharge rates over a long cycle life.

Besides these, some other studies showed that the electrochemical performance of V_2O_5 could be improved by introducing some guest cations (M) such as Ag^+, Cu^{2+}, Fe^{3+} and Cr^{3+} into the material matrix [9–13]. The improvement in electrochemical performance of the cation doped V_2O_5 has been attributed to their stabled crystal structure. Baffier and co-workers studied the structural properties of Fe^{3+} and Cr^{3+} doped V_2O_5 using X-ray diffraction [11,14]. It is revealed that the $[MO_6]$ octahedral in the doped materials link the V_2O_5 slabs, which increase the three-dimensional character of the material. This enhances the stability of the crystal structure and improves the electrochemical performance of the material. Raman scattering, which is much sensitive to the short-range environment of coordinative units, has been widely used in structural analysis. However, up to now there are limited works to study the local structure of cation doped V_2O_5 using Raman scattering. In this work, we prepared Al^{3+} doped V_2O_5 nanoparticles using an oxalic acid assisted soft-chemical method. We studied the effects of Al^{3+} doping on the structural properties of V_2O_5 using Raman scattering. In addition, the electrochemical properties of the material were compared with those of un-doped V_2O_5 nanoparticles with the aim to find a promising cathode material for rechargeable lithium batteries.

2. Experimental

For the preparation of Al^{3+} doped V_2O_5 nanoparticles, 0.01 mol of V_2O_5 (99%, Junsei) was dissolved in 100 ml of 0.3 mol L^{-1} oxalic acid solution. Afterwards, a 0.1 mol L^{-1} $Al(NO_3)_3$ was slowly titrated into the above solution until a molar ratio of Al:V = 1:10 was reached. The solution was stirred for 5–6 h at 80 °C, followed by drying at 100 °C to get a homogeneous precursor. This precursor was then subjected to heat treatment at 350 °C to obtain the final product. The preparation of V_2O_5 nanoparticles followed the same procedure as above but without using of the $Al(NO_3)_3$ solution.

Elemental analysis of Al and V was performed on an ICP-AES/1000 (PE Company) inductively coupled plasma instrument. The morphology features of the material were studied by scanning electron microscope (JEOL JSM-6700F). X-ray photoelectron spectroscopy (XPS) was performed on an ESCALAB spectrometer (VG scientific)

* Corresponding author. Tel.: +86 431 85155126; fax: +86 431 85155126.
E-mail address: yjwei@jlu.edu.cn (Y. Wei).

0925-8388/$ – see front matter © 2010 Elsevier B.V. All rights reserved.
doi:10.1016/j.jallcom.2010.03.133

using a monochromic Mg Kα excitation. The binding energy scale was corrected using the C 1s peak at 284.8 eV. X-ray diffraction data were collected on a Bruker D8 diffratometer with Cu Kα radiation. Raman scattering was performed on a Renishaw RM1000 micro-Raman instrument. The excitation light source was an Ar-ion laser with λ = 514.5 nm.

Electrochemical experiments were carried out using a two-electrode battery cell, using metallic lithium foil as the anodic electrode. The working electrode was composed of 75 wt.% of active material, 15 wt.% of carbon black and 10 wt.% of poly-vinylidenefluoride (PVDF) dissolved in *N*-methylpyrrolidone (NMP). The slurry mixture was spread on an Al foil and then dried in vacuum oven. The fabricated cathode electrode was cut into a size of 0.64 cm^2 (0.8 × 0.8). The electrolyte was a 1 M lithium perchlorate ($LiClO_4$) in 1:1 (v/v) ethylene carbonate/diethyl carbonate (EC/DEC). Galvanostatic charge–discharge cycling was carried out on a Land® (Wuhan) automatic battery cycler in the potential window of 4.0–2.0 V. Cyclic voltammetry was collected on a ZAHNER®-IM6e electrochemical workstation in the potential window of 4.0–2.0 V.

3. Results and discussion

3.1. Structural and morphology analysis

During the preparation of V_2O_5 nanoparticles, the V_2O_5 raw material was dissolved in oxalic acid solution. In the mean while, the solution color changed to blue. This occurred because oxalic acid is a reductive agent, which caused the reducing of V^{5+} to V^{4+} according to the following reaction,

$$V_2O_5 + 3H_2C_2O_4 \rightarrow 2[VO(C_2O_4)](\text{blue}) + CO_2 + 3H_2O$$

The V^{4+} ions have a typical color of blue. Subsequently, small clusters containing V^{4+} ions were formed during the reaction of V_2O_5 with oxalic acid. When the precursor was heat treated in air, the V^{4+} ions were oxidized to V^{5+} with the simultaneous decomposition of the precursor. This led to the formation of fine V_2O_5 nanoparticles which was confirmed by SEM as shown in Fig. 1(a). In addition, the SEM image of the Al^{3+} doped V_2O_5 (Fig. 1(b)) shows that the material was also composed of nano-sized particles, but with significant particle agglomeration. Elemental analysis determined that the molar ratio of Al:V of the material was close to 1:10.

Fig. 2 shows the V $2p_{3/2}$ XPS spectra of the as-prepared materials. The V $2p_{3/2}$ spectrum of the V_2O_5 sample was characterized by a single peak centered at 517.6 eV, which corresponds to the V^{5+} oxidation state [15]. The Al^{3+} doped sample showed a main peak at 517.6 eV, with a small shoulder at 516.3 eV. The later value fit well with that of V^{4+} in VO_2 [16]. This indicates that the vanadium ions in the material were in an intermediate oxidation state between V^{5+} and V^{4+}. The existence of V^{4+} ions was usually observed in cation doped V_2O_5 materials such as $Fe_{0.12}V_2O_{5.16}$, $Cu_{0.04}V_2O_5$ and $Ag_xV_2O_5$ gels [9,11,17]. Since it is difficult to determine the exact oxidation state of V in the material, we simplified the chemical composition of the Al^{3+} doped V_2O_5 as $Al_{0.2}V_2O_5$ in the following text.

Fig. 3 shows the X-ray diffraction patterns of the as-prepared nanoparticles. There were no apparent differences between the two diffraction patterns. This indicates that the crystal structure of $Al_{0.2}V_2O_5$ was close to that of orthorhombic V_2O_5, which was consistent with the previous report by Baffier et al. [18]. The lattice parameters of the materials were calculated based on the P_{mmn} space group, which were $a = 11.507(4)$ Å, $b = 3.565(1)$ Å, $c = 4.378(2)$ Å for V_2O_5 and $a = 11.511(3)$ Å, $b = 3.555(1)$ Å, $c = 4.359(3)$ Å for $Al_{0.2}V_2O_5$. The values in brackets are estimated standard deviations. The results indicate that the Al^{3+} dopant in V_2O_5 caused slight lattice expansion along the *a* axis and small compression along the *b* and *c* axis.

Fig. 4 displays the Raman patterns of the materials. There are three different V–O bonds in the V_2O_5 structure, i.e. the terminal V–O(1) bond, the chaining V–O(2) bond and the bridging V–O(3) bond [19]. As for the V_2O_5 nanoparticles, the Raman bands recorded

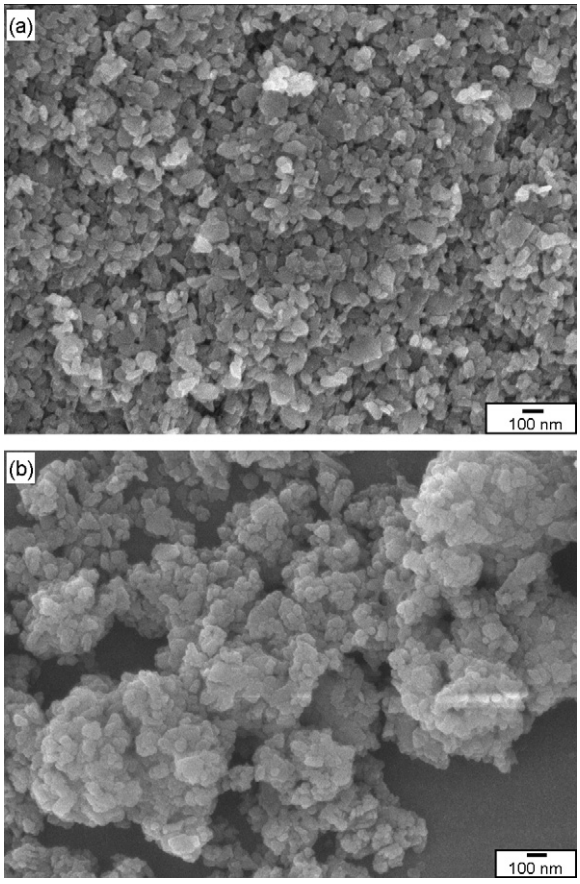

Fig. 1. SEM images of the (a) V_2O_5 and (b) $Al_{0.2}V_2O_5$ nanoparticles.

at 992, 691 and 527 cm^{-1} were assigned to the stretching modes of the V–O(1), V–O(3) and V–O(2) bonds, respectively. The bands located at 404 and 280 cm^{-1} corresponded to the bending modes of V–O(1), and those observed at 478 and 297 cm^{-1} were assigned to the bending modes of V–O(3) and V–O(2), respectively. There were two bands recorded at 191 and 140 cm^{-1}, which corresponded to the $[VO_5]$–$[VO_5]$ vibrations. These vibrations called as "external modes" reflected the cohesion between the V_2O_5 slabs.

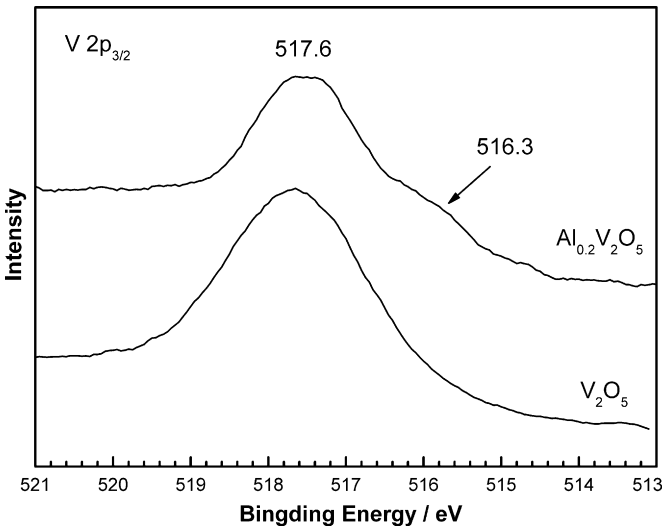

Fig. 2. V $2p_{2/3}$ XPS spectra of the V_2O_5 and $Al_{0.2}V_2O_5$ nanoparticles.

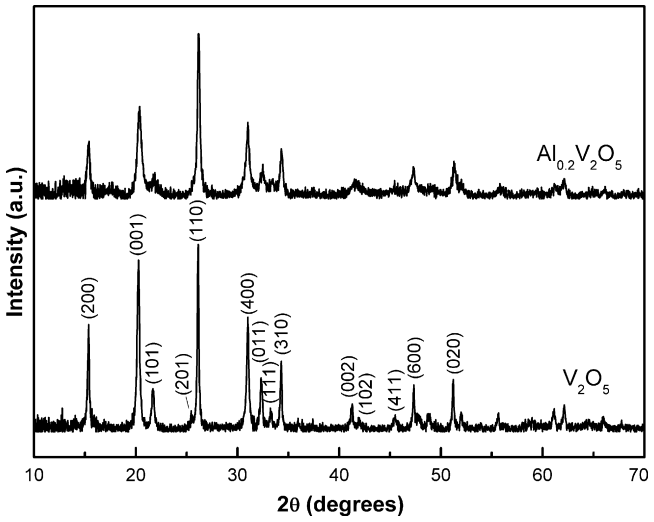

Fig. 3. X-ray diffraction patterns of the V_2O_5 and $Al_{0.2}V_2O_5$ nanoparticles.

It is very difficult to identify the Al–O vibrations from the Raman pattern of $Al_{0.2}V_2O_5$. However, we do observe a significant increase in the Raman intensity between 450 and 600 cm^{-1}. This could be due to the Al–O vibrations of the [AlO_6] octahedral [20], which were likely overlapped with the V–O vibrations. Most of the V–O bands of $Al_{0.2}V_2O_5$ located at the same wavenumbers as those of V_2O_5. However, the [VO_5]–[VO_5] vibration increased from 140 to 145 cm^{-1} after Al^{3+} doping, which indicates that the cohesion between the V_2O_5 slabs was strengthened by Al^{3+} doping. This also means that the structural stability of the material was enhanced by Al^{3+} doping. This would be good for the electrochemical performance of the material from the structural point of view. In addition, the V–O(3) stretching mode shifted from 691 to 701 cm^{-1}, corresponding to the softening of the V–O(3) bond. There were no obvious changes on the V–O(1) and V–(O2) vibrations. This indicates that the Al^{3+} cations did not significantly affect the V–O(1) and V–(O2) bonds.

3.2. Electrochemical properties

Fig. 5 shows the cyclic voltamgrams (CV) of the materials at different scan rates from 50 to 200 $\mu V\,s^{-1}$. Both materials exhibited three well-resolved redox couples, which are labeled as *a*/*a*′, *b*/*b*′ and *c*/*c*′, respectively. This indicates that the materials underwent

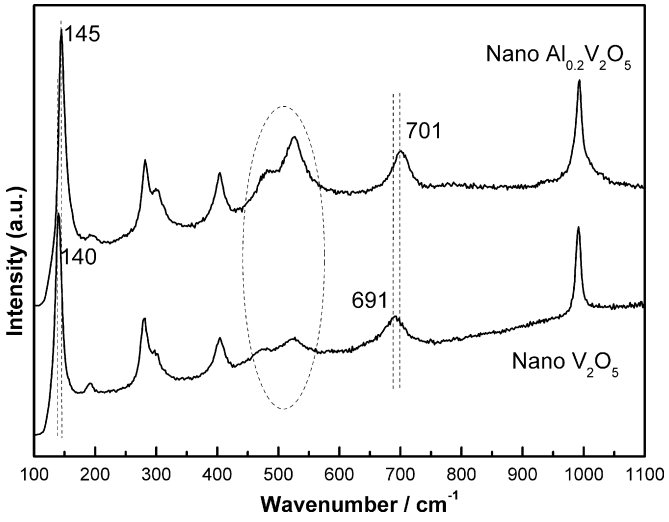

Fig. 4. Raman spectra of the V_2O_5 and $Al_{0.2}V_2O_5$ nanoparticles.

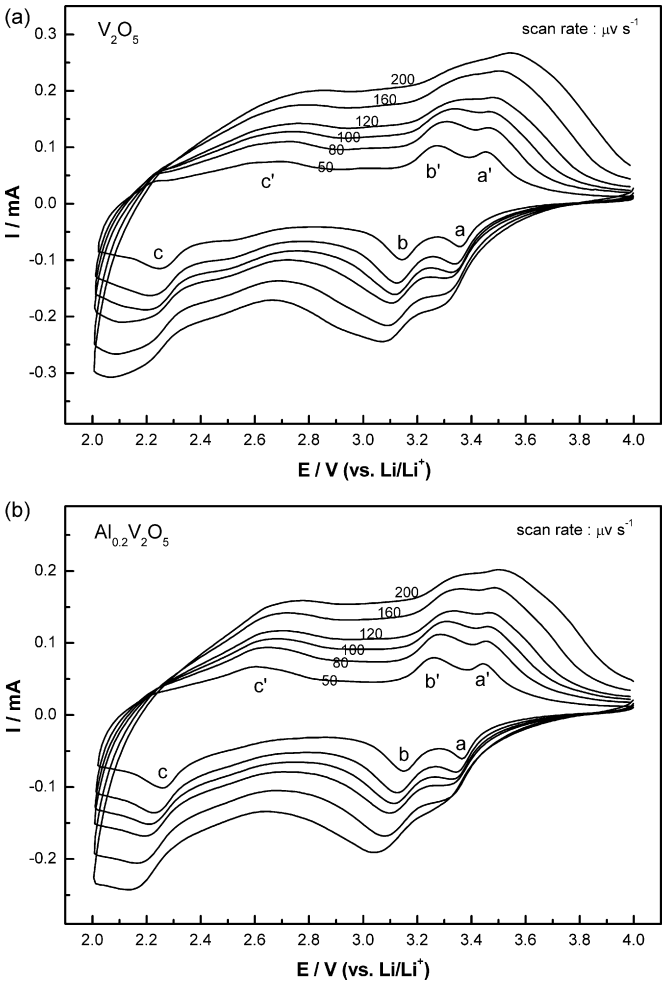

Fig. 5. Cyclic voltamgrams of the (a) V_2O_5 and (b) $Al_{0.2}V_2O_5$ nanoparticles.

reversible structural transitions during Li^+ insertion/extraction. The CV behavior of the V_2O_5 and $Al_{0.2}V_2O_5$ nanoparticles was different from that of crystalline bulk V_2O_5, which is known to experience irreversible structural transitions in the potential window of 4.0–2.0 V [21]. Recent studies have shown that these irreversible structural transitions can be effectively overcome by Cu^{2+} and Cr^{3+} doping [10,12]. The chemical diffusion coefficients of the materials, D_{Li}, can be evaluated from the CV measurements. In the case of semi-infinite diffusion, the peak current I_p can be expressed by the Randles and Sevcik equation [22,23]:

$$I_p = 2.687 \times 10^5 n^{3/2} \nu^{1/2} D_{Li}^{1/2} A C_{Li} \quad (1)$$

where n is the number of electrons per species reaction, ν the scan rate, A the electrode area, C_{Li} the Li^+ concentration in the electrode. Fig. 6 plots the I_p dependence on the scan rate of the CV measurement, from which I_p exhibited a linear relationship with the square root of scan rate ($\nu^{1/2}$). Using this relationship and the Eq. (1), the D_{Li} values of the V_2O_5 nanoparticles at the peak-*a*, -*b* and -*c* were calculated to be 7.0×10^{-10}, 3.8×10^{-11} and 2.1×10^{-12} $cm^2\,s^{-1}$, respectively. The corresponding values of the $Al_{0.2}V_2O_5$ nanoparticles were 2.6×10^{-10}, 2.4×10^{-11} and 9.6×10^{-13} $cm^2\,s^{-1}$, respectively, which were a little smaller than those of V_2O_5. This may be due to the Al^{3+} dopants, which block the Li^+ diffusion in the material lattice.

Galvanostatic charge–discharge cycling was carried out in the potential window of 4.0–2.0 V. Fig. 7 displays the typical charge–discharge profiles of the materials at the current density

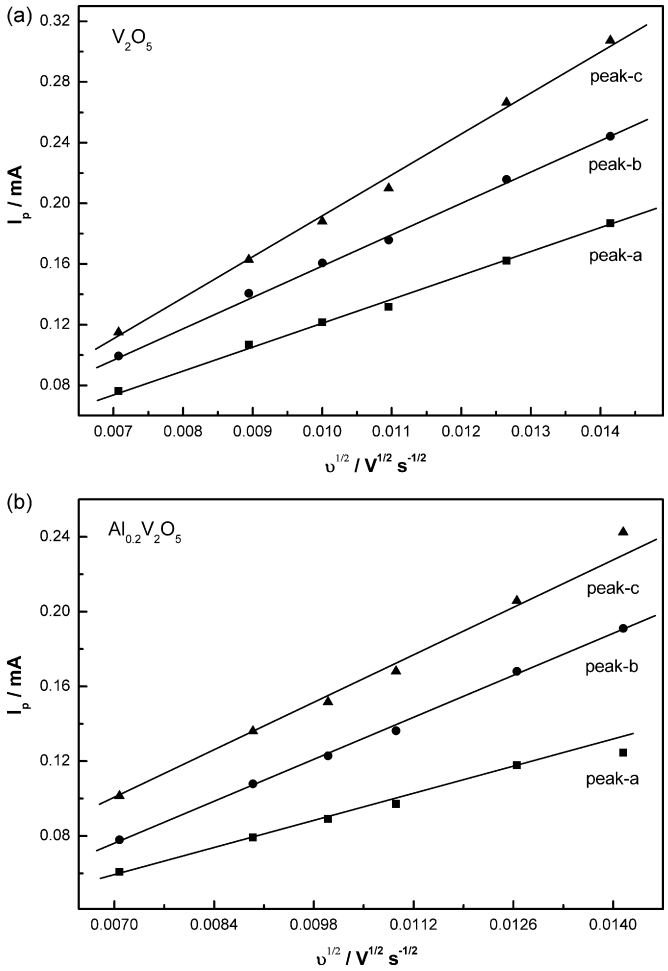

Fig. 6. The I_p *vs.* $\upsilon^{1/2}$ relationships of the (a) V_2O_5 and (b) $Al_{0.2}V_2O_5$ nanoparticles.

of 150 mA g^{-1}. Both materials showed three discharge plateaus at ~3.3, 3.1 and 2.3 V, which were consistent with the cyclic voltamgrams. However, the discharge plateaus of the $Al_{0.2}V_2O_5$ nanoparticles were much shorter than those of V_2O_5. In addition, a gradual potential decrease was observed between 3.1 and 2.3 V, in contrast to the abrupt decrease of the V_2O_5 nanoparticles. This suggests limited structural changes taken place in the $Al_{0.2}V_2O_5$ nanoparticles. Precise structural determinations should

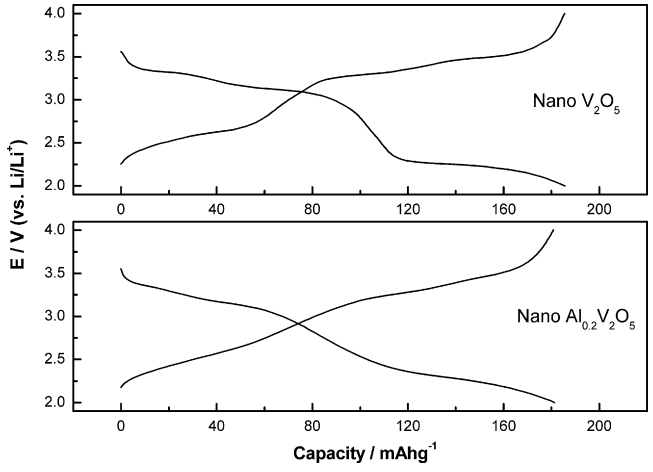

Fig. 7. Charge–discharge potential profiles of the V_2O_5 and $Al_{0.2}V_2O_5$ nanoparticles at the current density of 150 mA g^{-1}.

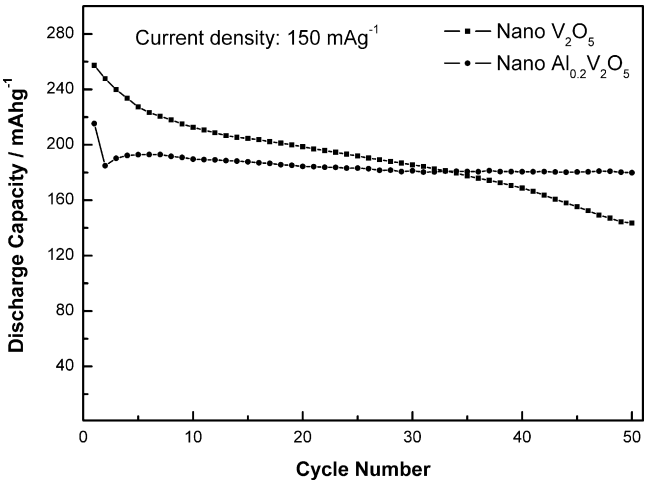

Fig. 8. Cycling performance of the V_2O_5 and $Al_{0.2}V_2O_5$ nanoparticles at the current density of 150 mA g^{-1}.

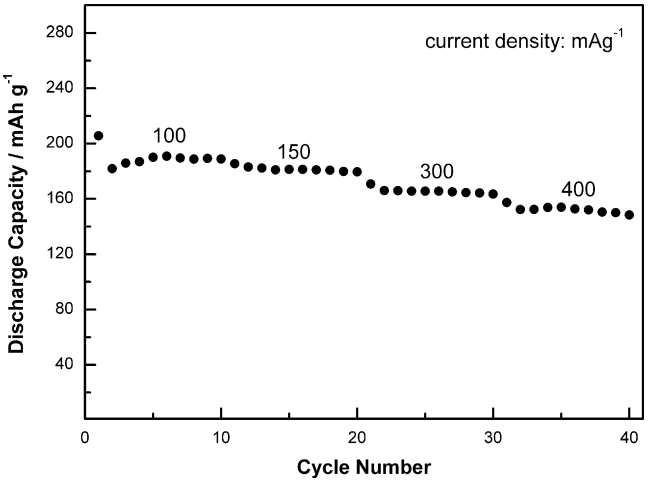

Fig. 9. Cycling performance of the $Al_{0.2}V_2O_5$ nanoparticles at different current densities from 100 to 400 mA g^{-1}.

be done to investigate the phase transitions of the materials during lithium intercalation. Fig. 8 shows the cycling performance of the materials. The initial discharge capacity of the V_2O_5 nanoparticles was ~260 mAh g^{-1}. The material showed continuous capacity fading, which dropped below 140 mAh g^{-1} after 50 cycles. The $Al_{0.2}V_2O_5$ nanoparticles exhibited a smaller discharge capacity of ~220 mAh g^{-1} in the first cycle. This was probably due to the additional Al^{3+} cations, which may occupy partial of the crystallographic sites that originally belong to Li^+. The material showed a capacity loss in the second cycle. However, it is exciting to see that the material showed rather good cycling stability with prolonged cycling. The discharge capacity was 180 mAh g^{-1} after 50 cycles, which exhibited almost no capacity fading with respect to the third cycle. In addition, the material exhibited good rate capability in that a reversible discharge capacity as high as 150 mAh g^{-1} was obtained when the current density increased to 400 mA g^{-1} (Fig. 9).

4. Conclusions

We have prepared V_2O_5 and $Al_{0.2}V_2O_5$ nanoparticles by a simple soft-chemical method. The $Al_{0.2}V_2O_5$ nanoparticles had an orthorhombic structure as that of V_2O_5. The Al^{3+} ions were bonded with oxygen in an [AlO_6] octahedral environment. The doping of Al^{3+} increased the cohesion between the V_2O_5 slabs, which

enhanced the structural stability of the material. Even though the chemical diffusion coefficients of $Al_{0.2}V_2O_5$ were a little bit smaller than those of the V_2O_5 nanoparticles, the doped material still showed better electrochemical performance, especially excellent capacity retention. The reason for the improved electrochemical performance by Al^{3+} doping was at least attributed to the enhancement in structural stability of the material.

Acknowledgements

This work was supported by MOST (No. 2009CB220104) and NSFC (No. 50702024). The authors thank the Program for Changjiang Scholar and Innovative Research Team in University (No. IRT0625) and the Program for New Century Excellent Talents (NCET-07-0366) for financial supporting.

References

[1] E. Baudrin, G. Sudant, D. Larcher, B. Dunn, J.-M. Tarascon, Chem. Mater. 18 (2006) 4369–4374.
[2] H.M. Zeng, Y. Zhao, Y.J. Hao, Q.Y. Lai, J.H. Huang, X.Y. Ji, J. Alloys Compd. 477 (2009) 800–804.
[3] Y. Chen, H. Liu, W.-L. Ye, Scripta Mater. 59 (2008) 372–375.
[4] X. Wei, L. Jiao, S. Liu, J. Sun, W.X. Peng, H. Gao, Y. Si, H. Yuan, J. Alloys Compd. 486 (2009) 672–676.
[5] J. Gao, J. Kim, A. Manthiram, Electrochem. Commun. 11 (2009) 84–86.
[6] W. Wu, Y. Wang, X. Wang, Q.Q. Chen, X. Wang, S.Y. Yang, X.M. Liu, J. Guo, Z.H. Yang, J. Alloys Compd. 486 (2009) 93–96.
[7] S.L. Chou, J.Z. Wang, J.Z. Sun, D. Wexler, M. Forsyth, H.-K. Liu, D.R. MacFarlane, S.-X. Dou, Chem. Mater. 20 (2008) 7044–7051.
[8] C.Q. Feng, S.Y. Wang, R. Zeng, Z.P. Guo, K. Konstantinov, H.K. Liu, J. Power Sources 184 (2008) 485–488.
[9] F. Coustier, S. Passerini, W.H. Smyrl, Solid State Ionics 100 (1997) 247–258.
[10] M. Giorgetti, M. Berrettoni, W.H. Smyrl, Chem. Mater. 19 (2007) 5991–6000.
[11] J. Farcy, S. Maingot, P. Soudan, J.P. Pereira-Ramos, N. Baffier, Solid State Ionics 99 (1997) 61–69.
[12] C. Leger, S. Bach, P. Soudan, J.-P. Pereira-Ramos, Solid State Ionics 176 (2005) 1365–1369.
[13] S.Y. Zhan, G. Chen, D.L. Liu, A. Li, C.Z. Wang, Y.J. Wei, J. Alloys Compd. 479 (2009) 652–656.
[14] G. Grégoire, N. Baffier, A. Kahn-Harari, J.-C. Badot, J. Mater. Chem. 8 (1998) 2103–2108.
[15] G. Bliznakov, Y. Pesheva, D. Klissurski, M. Marinov, V. Kozhukharov, Appl. Catal. 29 (1987) 211–218.
[16] T. Christmann, B. Felde, W. Niessner, D. Schalch, A. Schrmann, Thin Solid Films 287 (1996) 134–138.
[17] Y.J. Wei, C.W. Ryu, K.B. Kim, J. Power Sources 165 (2007) 386–392.
[18] N. Baffier, L. Znaidi, M. Huber, Mater. Res. Bull. 25 (1990) 705–713.
[19] R. Baddour-Hadjean, J.P. Pereira-Ramos, C. Navone, M. Smirnov, Chem. Mater. 20 (2008) 1916–1923.
[20] D.K. Breitinger, H.-H. Belz, L. Hajba, V. Komlósi, J. Mink, G. Brehm, D. Colognesi, S.F. Parker, R.G. Schwab, J. Mol. Struct. 706 (2004) 95–99.
[21] F.J. Anaissi, G.J.F. Demets, H.E. Toma, Electrochem. Commun. 1 (1999) 332–335.
[22] M.D. Levi, D. Aurbach, J. Electroanal. Chem. 421 (1997) 79–88.
[23] F. Wu, L. Wang, C. Wu, Y. Bai, Elctrochim. Acta 54 (2009) 4613–4619.